Pergamon

Int. J. Heat Mass Transfer. Vol. 40, No. 2, pp. 461–479, 1997

0017–9310/97 $15.00 + 0.00

PII: S0017–9310(96)00033–6

Developing and periodically developed flow, temperature and heat transfer in a ribbed duct

S. ACHARYA, T. MYRUM, X. QIU and S. SINHA

Mechanical Engineering Department, Louisianna State University, Baton Rouge, LA 70803, U.S.A.

(*Received* 7 *August* 1994 *and in final form* 19 *January* 1996)

Abstract—Measurements of the flow field and thermal field are reported for a flow in a periodically ribbed duct at two Reynolds number, 3400 and 24 000. At the lower Reynolds number, the incoming flow is transitional, while at $Re = 24\,000$, the incoming flow is fully turbulent. Thus, the reported measurements highlight the differences in the development of the surface heat transfer of a flow undergoing transition ($Re = 3400$) with that of a fully turbulent flow ($Re = 24\,000$) in a ribbed duct. At $Re = 3400$, the heat transfer in the first interrib module, due to the transitional nature of the flow, is lower than the heat transfer in the second interrib module. For the fully turbulent flow, the heat transfer profile in successive interrib modules decays to the periodic state. Associated velocity measurements confirm the transitional behavior at $Re = 3400$, with nearly a twofold increase in the normalized streamwise velocity fluctuations past the first interrib module, where transition is completed. At $Re = 24\,000$, no such dramatic increases of streamwise turbulence levels is noted. The detailed set of measurements provides a complete picture of the transitional and fully turbulent flow and heat transfer in a ribbed duct. Copyright © 1996 Elsevier Science Ltd.

INTRODUCTION

Turbulent flow and heat transfer in ribbed ducts are of interest in a variety of applications, including internal cooling of gas turbine blades, internally ribbed heat exchangers and electronic cooling. While there is an extensive body of literature dealing with flow and heat transfer in ribbed ducts, the majority of the reported studies deal with high Reynolds number turbulent flow. Furthermore, detailed measurements of velocity and temperature fields in the near-rib regions of both the developing and periodically developed regions are somewhat limited.

The objective of this study is to report detailed measurements of the velocity, temperature, and heat transfer in both the developing and periodically developed regions of a ribbed duct. Flows at two Reynolds numbers (Re) are considered. In the first case, the Re, based on the hydraulic diameter, is approximately 3400, and the flow at the inlet to the ribbed test section is transitional. In the second case ($Re = 24\,000$) the incoming flow is fully turbulent. There are significant differences in the development of the Nusselt number profiles between the incoming transitional flow case and the incoming fully turbulent case. The detailed measurements presented in this paper help explain these differences. Further, the present paper provides a clearer picture of the simultaneous flow and temperature development in a heated ribbed duct. Reported studies are generally either purely hydrodynamic studies or focus on the heat transfer issues.

A number of investigators have performed 'cold'-flow studies of turbulent flow past successive ribs. Durst *et al.* [1] reported laser-Doppler velocimeter (LDV) measurements of fully developed turbulent channel flow with two ribs mounted in succession. Liou *et al.* [2] performed measurements of mean velocity and turbulence intensity for flow past two pairs of turbulence promoters in the Re range of 12 000–120 000. This study was followed by LDV measurements at $Re = 33\,000$ in a channel with ribs on opposite walls [3]. Drain and Martin [4] and Yokosawa *et al.* [5] also report fully developed flow measurement in a rib-roughed channel. More recently, Acharya *et al.* [6] have made detailed LDV measurements of the fully developed turbulent flow field in a ribbed duct at $Re = 24\,000$. They also report detailed temperature and heat transfer measurements.

In addition to ref. [6], a number of other studies report heat transfer measurements in a ribbed duct. Lockett and Collins [7] report holographic interferometric measurements in a ribbed channel and present Nusselt numbers in the Re range of 10 000–30 000. Sparrow and Tao [8] and Han *et al.* [9, 10] have also reported measurements for fully turbulent flow in a ribbed channel. Liou and Hwang [3, 11] and Liou *et al.* [12] have made holographic interferometer measurements and deduced the Nusselt number in the Reynolds number range of 5000–54 000. Their results for the entire Re range indicates that the flow at the inlet to the test section was turbulent. More recently, Aiaga *et al.* [13] have made heat transfer measurements using an infrared thermography technique in a channel with square ribs. The Reynolds numbers considered were 500 000 and higher.

As noted above, the majority of the literature deals with fully turbulent flows, and little or no information

NOMENCLATURE

A_s surface area of the heated shim
D_h hydraulic diameter of test section
Gr_H Grashof number based on channel height
h rib height
h_c heat transfer coefficient, $q_c''/(T_s - T_b)$
H channel height
k thermal conductivity of air at inlet temperature
Nu Nusselt number, $h_c D_h/k$
q total power input to shim
q_c'' convective heat flux from shim
Re, Re_H Reynolds number based on hydraulic diameter and channel height, respectively, $Re = U_0 D_h/v$, $Re_H = U_0 H/v$
T, T_{in}, T_b, T_s temperature, inlet temperature, bulk temperature and shim temperature, respectively
u, v velocity components in the x- and y-directions, respectively
u', v' velocity fluctuation in u and v
U_0, u_τ mean velocity and friction velocity, respectively
U^+ dimensionless velocity, u/u_τ
x, y coordinate in the streamwise and cross-stream directions, respectively
x' x-distance measured from the downstream face of each rib
Y^+ dimensionless coordinate, yu_τ/v.

Greek symbols
δ boundary layer thickness
v kinematic viscosity
τ_w wall shear stress.

is available in the transitional-Re regime. In this paper, measurements are reported for both initially-transitional and full turbulent flows. These measurements include the simultaneously developing velocity, temperature and heat transfer fields.

THE EXPERIMENTS

The experimental setup and flow measurement system are shown schematically in Fig. 1(a). Details of the test section are shown in Fig. 1(b). Air was drawn into the development section of the wind tunnel through a 5.25-to-1 contraction section containing a honeycomb baffle and four screens. Velocity measurements at the exit to the contraction section indicate a virtually uniform velocity profile. The test section, 101.6 cm long, 30 cm wide and 6.1 cm high was placed 40 hydraulic diameters downstream of the inlet. Eight steel ribs, each with a 6.35×6.35 mm square cross-section were attached to the lower wall using double-sided tape, and were uniformly spaced with a pitch to rib height ratio of 20.

The flow measurements were made using a conventional two-component DANTEC fiber-optic LDV system operating in the backscatter mode. Each measurement consisted of nearly 3000 samples at each location recorded at a sampling rate that varied from 25 samples s^{-1} in the near-wall recirculating region to 1500 samples s^{-1} in the outer edge of the shear layer. Sample size measurements ranging from 2000 to 10 000 were performed at various locations with less than a 1% difference in the mean and r.m.s. values. Ensemble averaging, without two-dimensional velocity bias correction, was used to calculate the mean velocity and turbulent stresses. As pointed out by Driver and Seegmiller [14, 15], two-dimensional bias corrections in a recirculating flowfield are inappropriate, since the data corresponding to a very low or zero u- and v-velocity is weighted with an extremely high weight factor which, in a strongly turbulent flowfield with a significant w'_{rms} component, would be incorrect. For a backstep flow, Driver and Seegmiller [14] made three-dimensional velocity bias corrections and found changes in the mean velocity and Reynolds stresses that were less than 5% of the maximum measured levels. The uncertainties were calculated to a 95% confidence level, as recommended by Kline and McClintock [16] and Rood and Telionis [17], and are found to be ± 3.5 and $\pm 3\%$ for the mean u- and v-velocities, ± 5 and $\pm 4.5\%$ for the streamwise and cross-stream turbulence intensities, and $\pm 8\%$ for the turbulent shear stress.

For the heat transfer experiments, a 0.025-mm thick stainless steel shim was epoxied to the bottom wall of the test section, and a constant heat flux boundary condition was simulated by passing direct current through it. Eight balsa-wood ribs, 6.35×6.35 mm square, were distributed uniformly on the shim surface, exactly as in the 'cold'-flow study. The entire test section was engulfed in fiberglass insulation to minimize conduction losses.

For surface temperature measurements, chromel–constantan thermocouples (0.076 mm in diameter) were spot-welded to the bottom of the shim at 5.1 mm intervals along the centerline. To measure spanwise temperature variations, a few thermocouples were

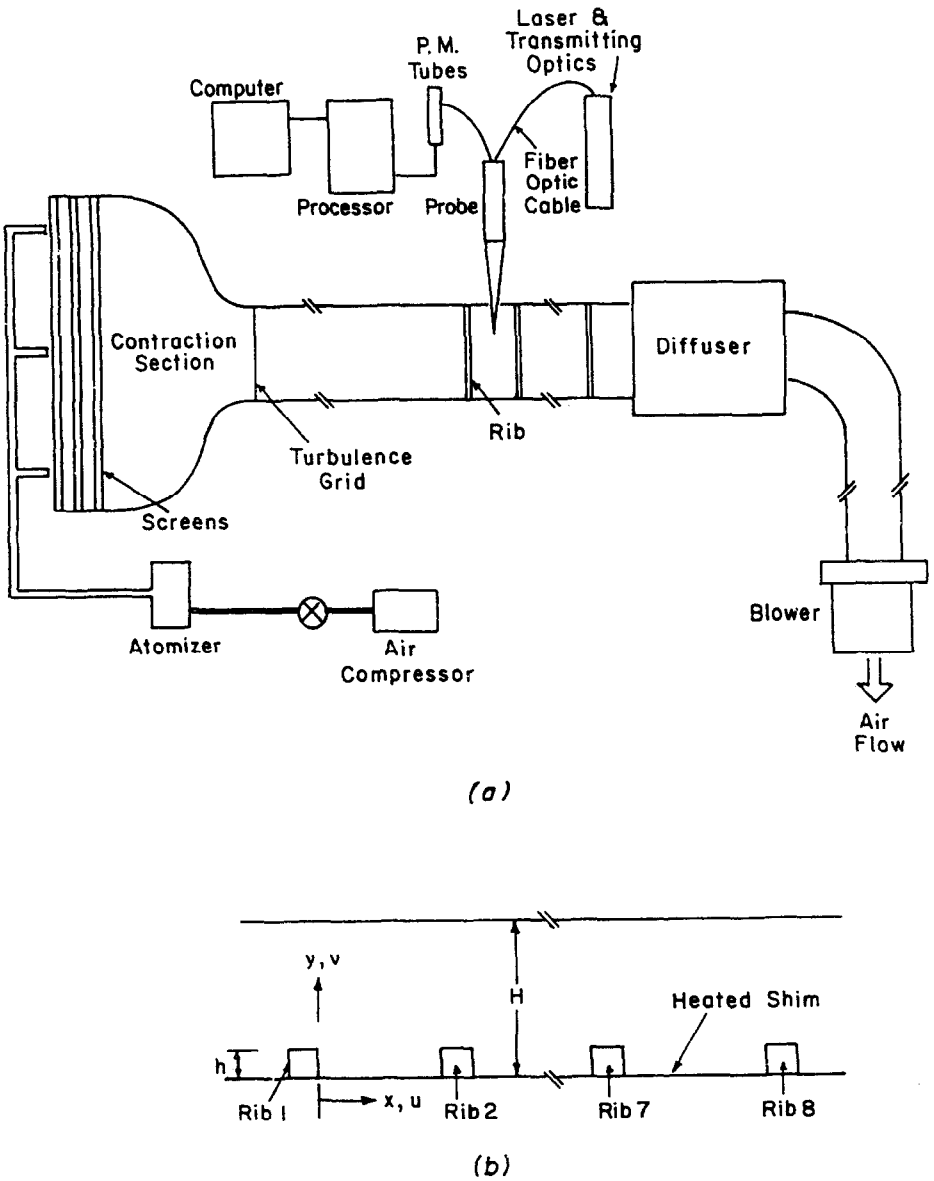

Fig. 1. (a) Experimental facility, (b) schematic of the test section.

positioned at off-centerline locations, and indicated a spanwise variation of less than 6% of the minimum shim-to-bulk fluid temperature difference.

Surface heat transfer results are presented in the form of local Nusselt number values, and these are calculated from the convective heat flux, the measured shim temperatures, and the bulk temperatures. The convective heat flux is determined by subtracting conduction and radiation heat losses from the local electric heat flux generation, that is determined from measurements of the current supplied to the shim and its temperature dependent electrical resistivity. To calculate conduction heat losses, a finite difference code was used to solve the heat conduction equation in the insulating region below the shim with the measured temperatures along the shim and along the side and bottom walls of the insulation below the test section as input boundary conditions. Conduction and radiation heat losses were less than 5% of the local electric heat flux generation. The uncertainty in the local Nusselt number, obtained with the above procedure, was found to be $\pm 5\%$.

All measurements were taken after steady state was achieved. For the velocity measurements steady conditions were established relatively quickly, while for the heat transfer study, it took several hours for steady-state conditions to be reached. The buoyancy parameter (Gr_H/Re_H^2) was less than 0.002, where Gr_H and Re_H are the duct-height-based Grashof and Reynolds number, respectively. Thus, the buoyancy effects were negligible.

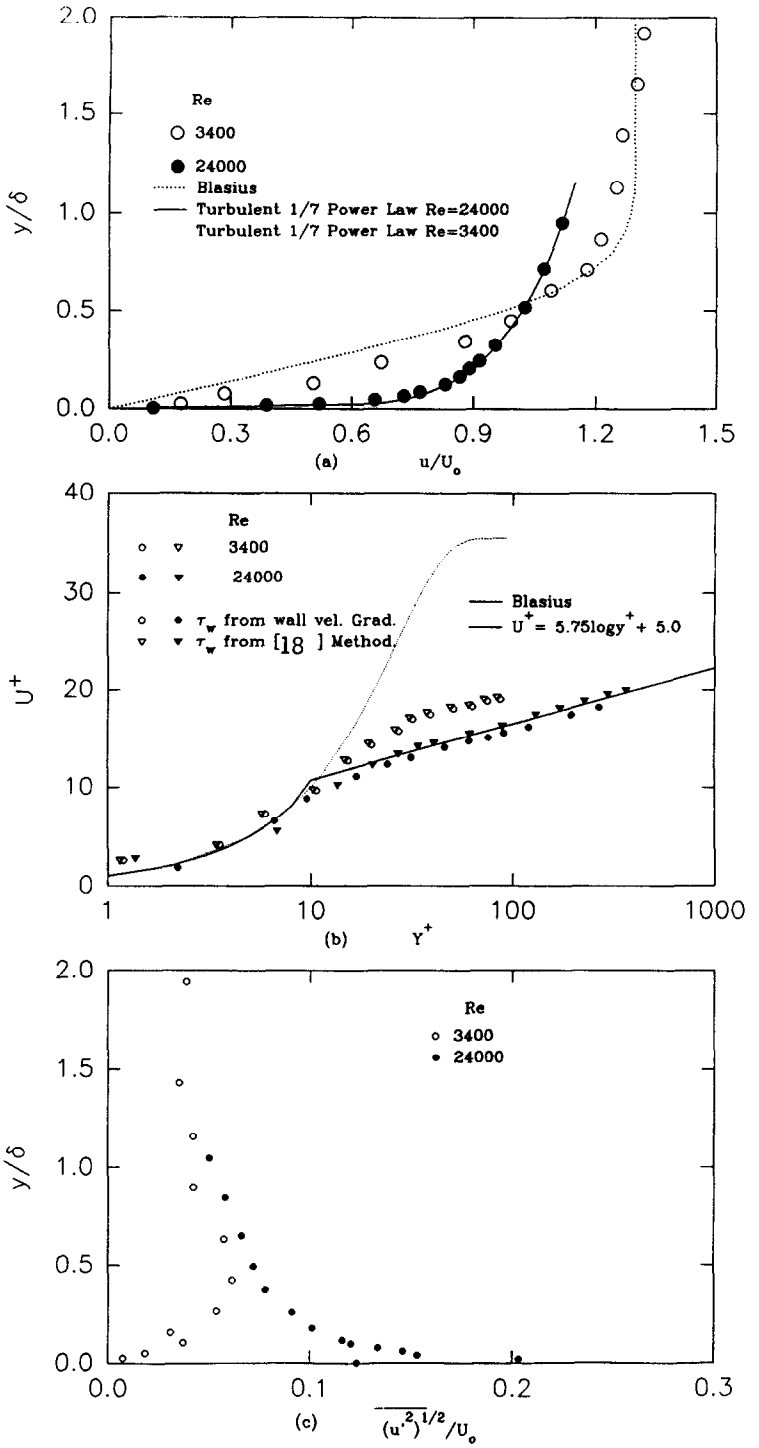

Fig. 2. Velocity and turbulence intensity profiles at the inlet to the smooth test section: (a) streamwise velocity profiles; (b) velocity profiles in law-of-the-wall coordinates; (c) streamwise turbulence intensity profiles.

RESULTS AND DISCUSSION

Incoming flow

The velocity profile upstream of the test section was measured to determine inlet flow conditions. Figure 2(a) presents the measured velocity profiles at $Re = 3400$ and 24000. Also shown are the laminar Blassius profile at $Re = 3400$ and the turbulent one-seventh power law profile at $Re = 24000$. The measured velocity profile at $Re = 24000$ fits the (1/7)th power law profile quite well, indicating that the flow is fully turbulent. The same observation can be made by plotting the profiles in log-law-coordinates, as shown in Fig. 2(b). To calculate the wall shear stress,

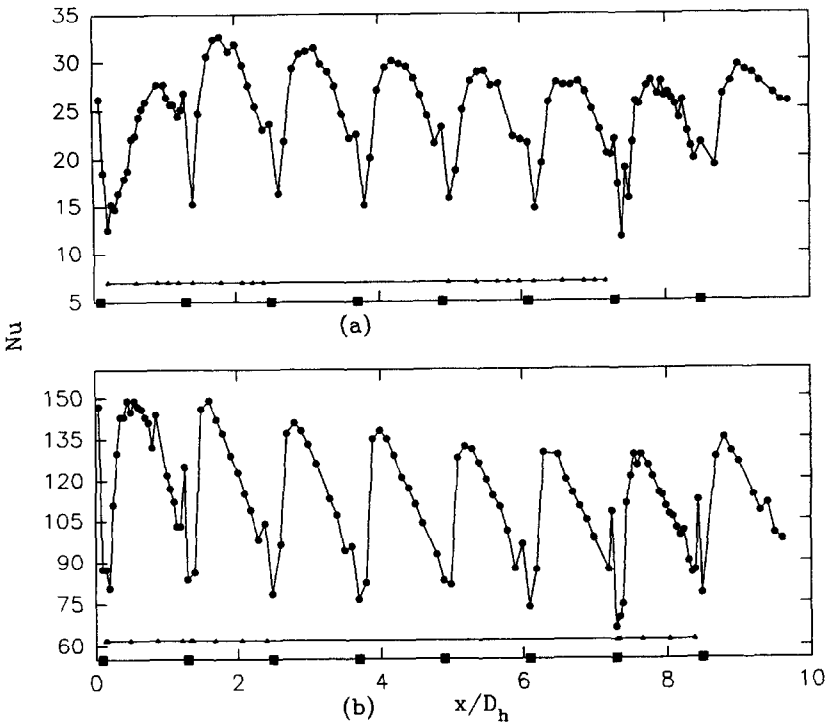

Fig. 3. Nusselt number profiles in the ribbed test section: (a) $Re = 3400$; (b) $Re = 24000$. (Dark square symbols indicate location of ribs, dark triangle symbols indicate location of temperature profiles.)

two methods were used. One was to compute it directly from the measured velocity gradient at the wall and the other method was based on the approach of Cole and Hurst [18], where the wall shear was computed using the Ludwieg–Tillman formula, and then adjusted to minimize deviations of the measured values from the log-law profile. Both methods give fairly close values. Measured profiles at $Re = 24000$ appear to fit the law of the wall and the log law profiles quite well. For the lower Reynolds number ($=3400$), the measured data points lie in-between the Blassius profile and the log-law profile, indicating a transitional state.

Measured turbulence intensities are presented in Fig. 2(c). As expected, the peak turbulence levels at $Re = 24000$ are much higher (nearly four times) and occur much closer to the wall than at $Re = 3400$. In the free stream, the turbulence levels decay, and at $Re = 24000$, they are only 20% higher than the intensity level at $Re = 3400$.

Heat transfer measurements

The Nusselt number profiles at $Re \cong 3400$ and $Re \cong 24000$ are shown in Fig. 3. The location of the ribs are indicated on the horizontal axis by the filled squares. Each point on the Nusselt number plot represents a thermocouple location. Note that in the heat transfer experiments, the ribs are made from balsa wood, are nonconducting, and therefore correspond to a local minimum in the Nusselt number profiles. The use of balsa wood ribs implies that the Nusselt numbers represent the manifestations of the flowfield alone and are not distorted by rib-conduction effects. Two local maxima can be seen in each interrib module, with the larger peak occuring in the vicinity of the reattachment downstream of the rib, and a smaller peak occuring immediately upstream of the rib, due to a small counter-rotating eddy in the rib upstream corner. The heat transfer peak upstream of the rib has been noted by several researchers (see ref. [8], for example) and has been linked to the upstream separated eddy measured in several studies, including that of Acharya *et al* [19] for flow past a single rib.

Consider first the $Re = 24000$ case [Fig. 3(b)], for which the incoming flow is fully turbulent. The successive interrib profiles exhibit the expected decay in the *Nu*-values, until they reach a periodically fully developed state. The interib profiles in the fifth, sixth, and seventh interrib modules are nearly identical, indicating the periodically developed condition. Note that immediately upstream of the rib, the *Nu*-peak is relatively sharp, due to the small size of the upstream corner eddy, and therefore, the resolution of the upstream rib peak is extremely sensitive to the thermocouple placement. This is probably the reason why there are differences in the local peaks in the immediate vicinity of the rib in the periodically developed modules. Note that in the first and seventh interrib modules, the thermocouple resolution is nearly twice that in the other interrib modules. At this Reynolds number, the peak *Nu* location in each interrib module seems to be quite consistent, with a x/D_h value that shows a marginal decrease after the first module, but is generally in the range of 4.3 ± 0.8 for all seven modules.

The development of the Nusselt number profiles at $Re = 3400$ [Fig. 3(a)], is remarkably different than that just described at the higher Reynolds number. The Nusselt number profile in the first interrib module is lower than the corresponding profile in the second interrib module, beyond which the successive interrib profiles exhibit the expected decay to the periodic state. The rather unexpected and heretofore unreported increase in the Nusselt number values between the first and second interrib modules, is due to the transitional state of the incoming flow, as shown in Fig. 2. There is a significant increase in the turbulence intensity between the first and second interrib modules (as will be seen later). Thus, the Nusselt numbers in the first interrib module are smaller than the fully turbulent Nusselt numbers in the second interrib module, with the peak to peak increase at nearly 20%. Also, the Nusselt number peak in the first interrib module occurs substantially further downstream (at $x'/h \cong 13.1$) than in the second and subsequent interrib modules (at $x'/h \cong 7.5$). This is expected, since for turbulent flows, the eddy diffusivity and the growth of the separated shear layer is larger, and the reattachment length is shorter than for laminar/transitional flows. This observation will be further confirmed when evaluating the mean velocity profiles.

Temperature measurements

Temperature profiles were measured at x'/h locations between 1.1 and 17.1 in the first, second, fifth, and sixth interrib modules at $Re = 3400$, and in the first, second and seventh interrib module at $Re = 24\,000$. The x/D_h locations where the temperature profiles were measured are indicated in the Nusselt number plot (Fig. 3) by black triangles on an axis just above the horizontal axis of the plot.

Figure 4 shows the nondimensional temperature profiles at $Re = 3400$. The dimensionless wall temperature values, measured by the thermocouples below the shim surface are indicated in the horizontal axis. In the first interrib module [Fig. 4(a)], the separated temperature shear layer, due to its transitional nature, is considerably thinner in the transverse direction than in subsequent modules. Note that the separated shear layer exhibits an inflexional profile, and in the first interrib region, at $x'/h = 7.5$, the profile indicates the presence of the separated shear layer, while at $x'/h = 7.5$ behind subsequent ribs, the temperature profile indicates a reattached developing boundary layer profile.

The measured surface temperatures, indicated on the horizontal axis, correlate inversely with the local Nusselt number; that is, the peak Nu value corresponds to the lowest shim temperature. For a uniform heat flux (UHF) surface, this is the expected behavior. Note that in the second and subsequent interrib modules, the minimum in the shim temperature occurs at $x'/h = 7.5$, the location corresponding to the Nu peak in Fig. 2(a). In the first interrib module, consistent with the downstream shift in the Nu-peak in Fig. 2(a), the shim temperature at $x'/h = 12.3$ is lower than the corresponding values at the other four x'/h locations shown in the figure.

At $Re = 24\,000$ (Fig. 5), the temperature profiles in successive interrib modules have similar shapes. Near $x'/h = 5.7$, the shim temperature in each module shows the characteristic drop associated with reattachment and Nu peak. Thus, unlike the behavior noted at the lower Re, the measured thermal field in successive interrib modules have similar characteristics, and as indicated in the Nusselt number plot [Fig. 2(b)], develop in the expected manner to the periodic state.

Velocity measurements

The mean velocities and the turbulent stresses are presented in Figs. 6–10 for the lower Reynolds number, and in Figs. 11–15 for $Re = 24\,000$. For the lower Reynolds number, since the flow undergoes transition after interrib module 1, velocity and turbulence profiles are presented in interrib modules 1, 2, 5 and 6. At the higher Reynolds number, since the flow is fully turbulent over the entire ribbed test section, velocity measurements are only shown in interrib modules 1 and 7.

Figure 6 shows the mean velocity profiles at $Re = 3400$. Between ribs 1 and 2 [Fig. 6(a)] the flow at $x'/h = 7.5$ indicates the presence of a reversed flow region near the wall extending up to nearly half the rib height, while at $x'/h = 12.3$, the flow is entirely in the positive direction. Reattachment, therefore, occurs for an x'/h value between 7.5 and 12.3. However, in the second and subsequent interrib modules, the velocities at $x'/h = 7.5$ are all positive, and reattachment occurs for x'/h between 3.1 and 7.5. It is well known that the reattachment length for a turbulent separated shear layer, due to greater cross-stream turbulent diffusion, is smaller than the reattachment length for a laminar or transitional separated shear layer. This decrease in reattachment location between interrib modules 1 and 2 is, therefore, due in part, to the different flow regimes in the two modules, with that in module 1 being transitional, and that in module 2 being turbulent. Another factor that could also contribute to a shift in the reattachment location between the first two modules is the streamline curvature of the incoming flow.

The above noted observations regarding transition are further confirmed by the streamwise turbulence intensity profiles shown in Fig. 7. At about one rib-height downstream of separation ($x'/h = 1.1$), the peak streamwise turbulence intensity behind the first rib is nearly 0.2 and increases to nearly twice this value at the same location behind the second rib. The streamwise turbulence levels in the recirculation region behind the first rib are substantially smaller than the corresponding values behind the second rib, which is indicative of low values of cross-stream turbulent diffusion or eddy diffusivity immediately behind the

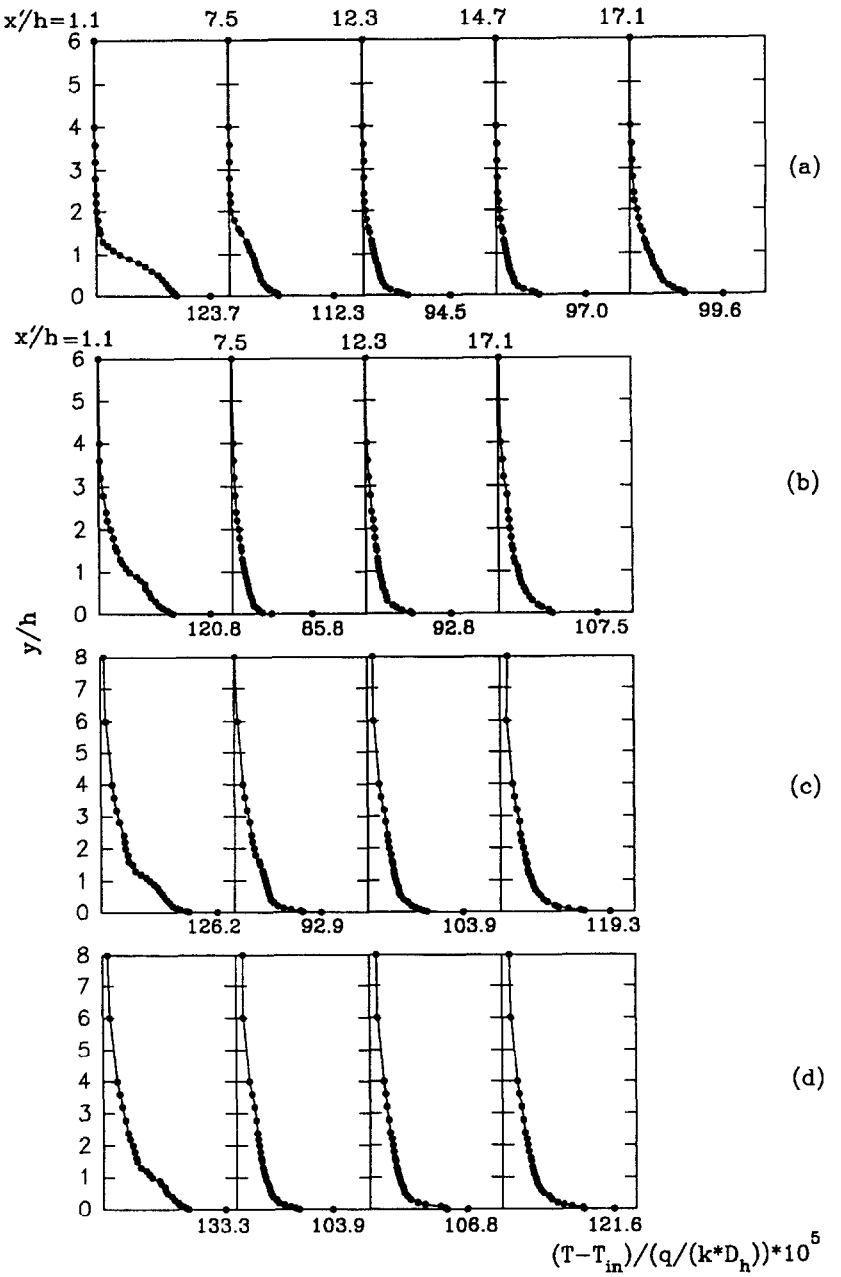

Fig. 4. Mean temperature profiles at $Re = 3400$: (a) between ribs 1 and 2; (b) between ribs 2 and 3; (c) between ribs 5 and 6; (d) between ribs 6 and 7.

first rib. Note that in the second and subsequent interrib modules there is a reduction in the turbulence levels past the location of peak turbulence. This behavior is consistent with previously reported measurements of turbulent flow past a single rib [19] or past a back step [20]. In the first interrib module, however, the near-wall turbulence values at $x'/h = 7.5$ increase substantially to about the same levels as observed in the second and subsequent interrib modules. This would, therefore, indicate that the flow becomes turbulent in the vicinity of the flow reattachment in the first interrib module.

The cross-stream velocity profiles are shown in Fig. 8, and are consistent with the features of the flow field noted above. In the downstream recirculation region, the v velocity is positive (upward) near the wall, and negative (downward) in the separated shear layer. In interrib module 1 evidence of the recirculation eddy is noticeable at $x'/h = 7.5$, while in subsequent modules, the v velocities are entirely negative at $x'/h = 7.5$,

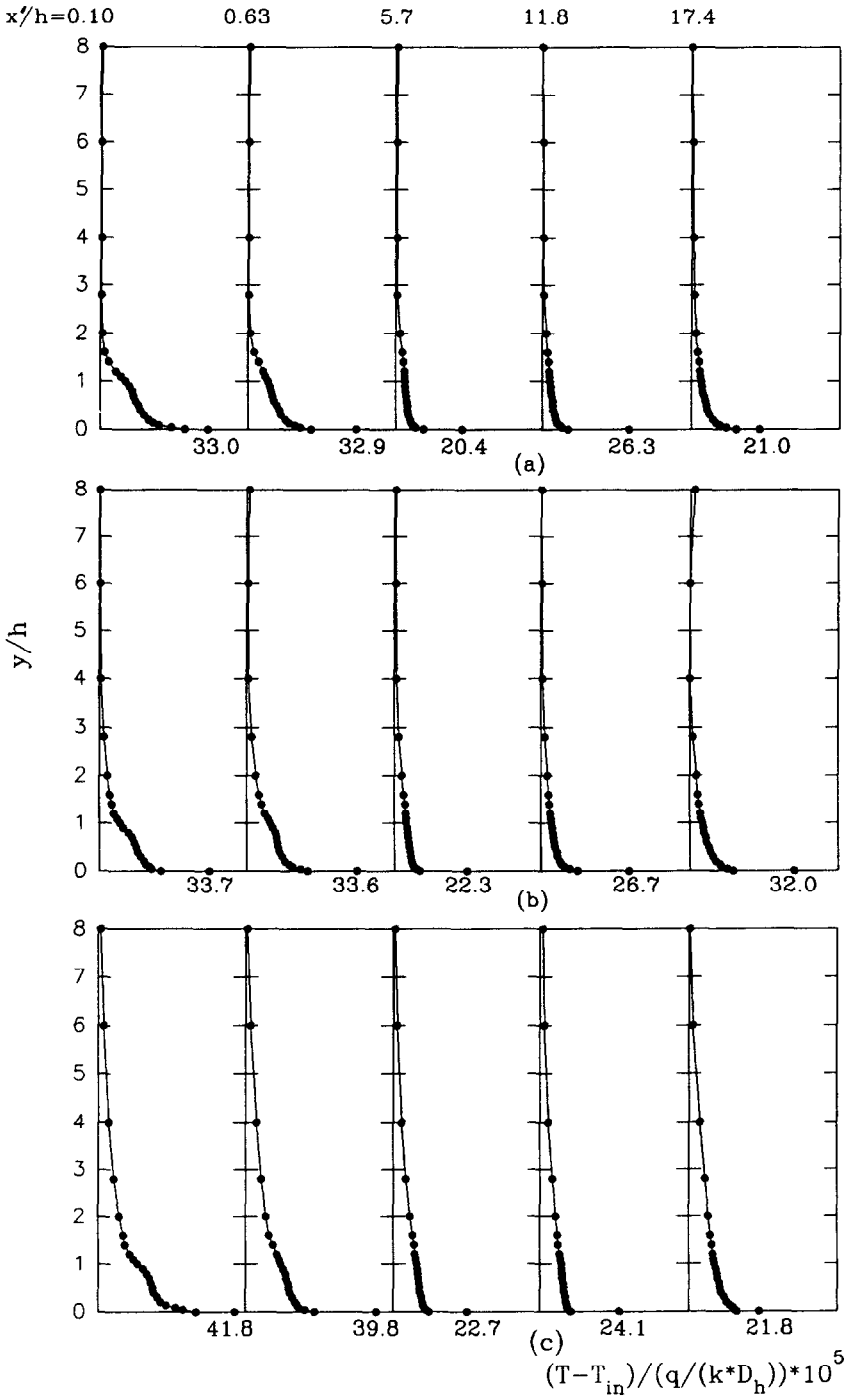

Fig. 5. Mean temperature profiles at $Re = 24\,000$: (a) between ribs 1 and 2; (b) between ribs 2 and 3; (c) between ribs 7 and 8.

indicative of a reattached, developing shear layer. At $x'/h = 14.7$, the v velocities in all modules are still negative, indicative of the persistence of the shear layer wake. At $x'/h = 17.1$, the separation induced by the downstream rib causes the flow to deflect upwards resulting in positive v velocities. The magnitudes of these positive velocities are comparable to the magnitudes of the v velocities in the separated region behind the ribs.

The cross-stream turbulence intensities (Fig. 9) are generally smaller than the streamwise intensities indicating the nonisotropic nature of the flow. In interrib

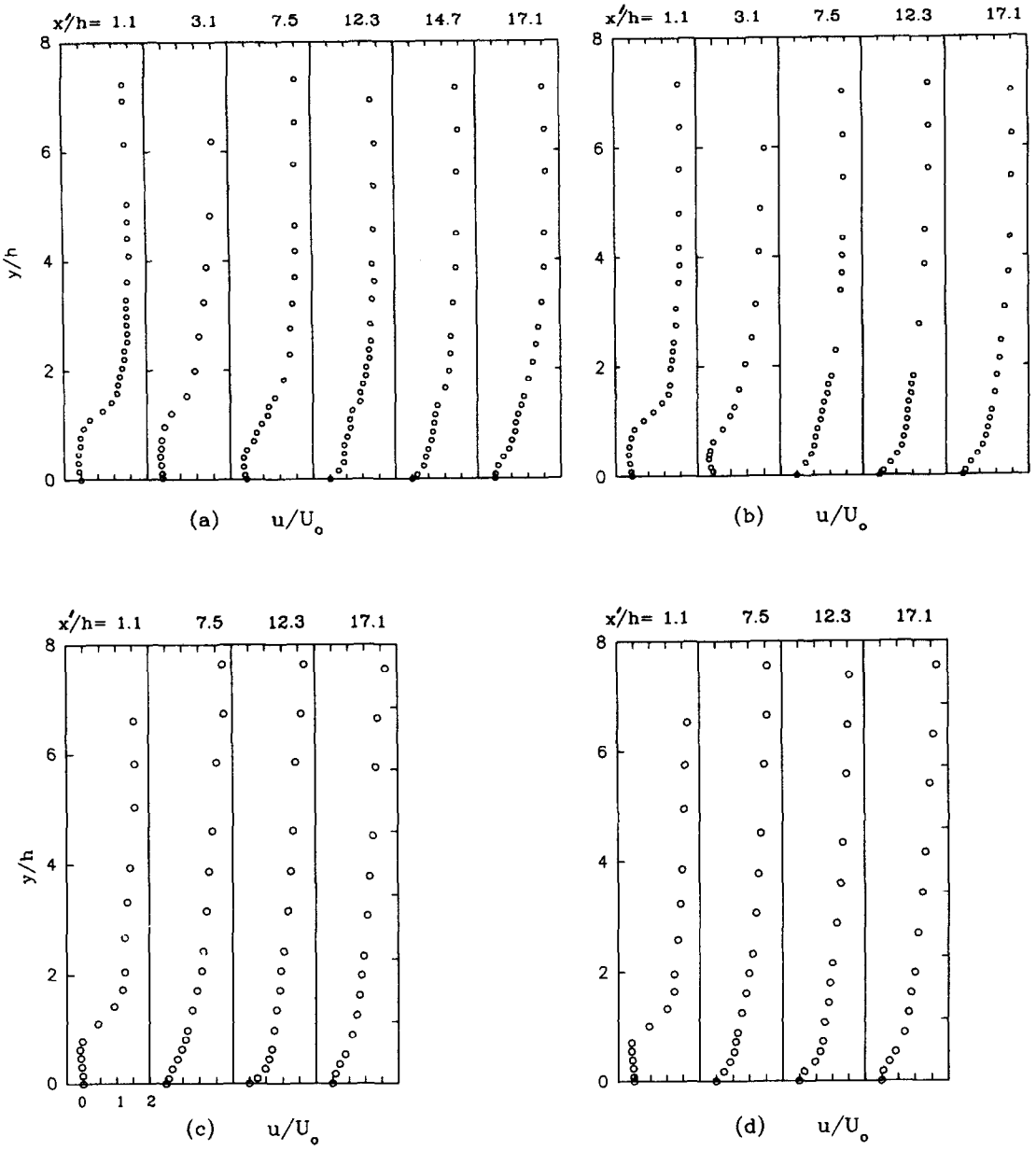

Fig. 6. Mean streamwise velocity profiles at $Re = 3400$: (a) between ribs 1 and 2; (b) between ribs 2 and 3; (c) between ribs 5 and 6; (d) between ribs 6 and 7.

module 1, the peak values are different by a ratio in the 1–1.5 range. In interrib module 2, where the flow is entirely turbulent, the ratio changes to nearly 2.5 at $x'/h = 1.1$ to 2.0 at $x'/h = 3.1$, and to about 1.5 further downstream. Clearly as the flow undergoes transition to fully turbulent flow, the production of the cross-stream turbulence lags behind the production of streamwise turbulence intensity, and the cross-stream turbulence increases by a relatively smaller proportion from a typical peak of 0.15 in the module 1 to a typical peak of 0.2 in modules 5 and 6.

The shear stress profiles are shown in Fig. 10, and indicate very small values in the recirculation regions. The near-wall values increase significantly in the vicinity of reattachment. The shear stresses just downstream of the second rib shows an increase by a factor of nearly 1.5 over the corresponding values past the first rib.

At the higher Reynolds number of 24000, the incoming flow is fully turbulent, and the streamwise profiles (Fig. 11) show the expected development of turbulent flow in a ribbed duct. Between ribs 1 and 2, reattachment occurs at an x'/h just downstream of 5.7, while in the periodically developed region, the

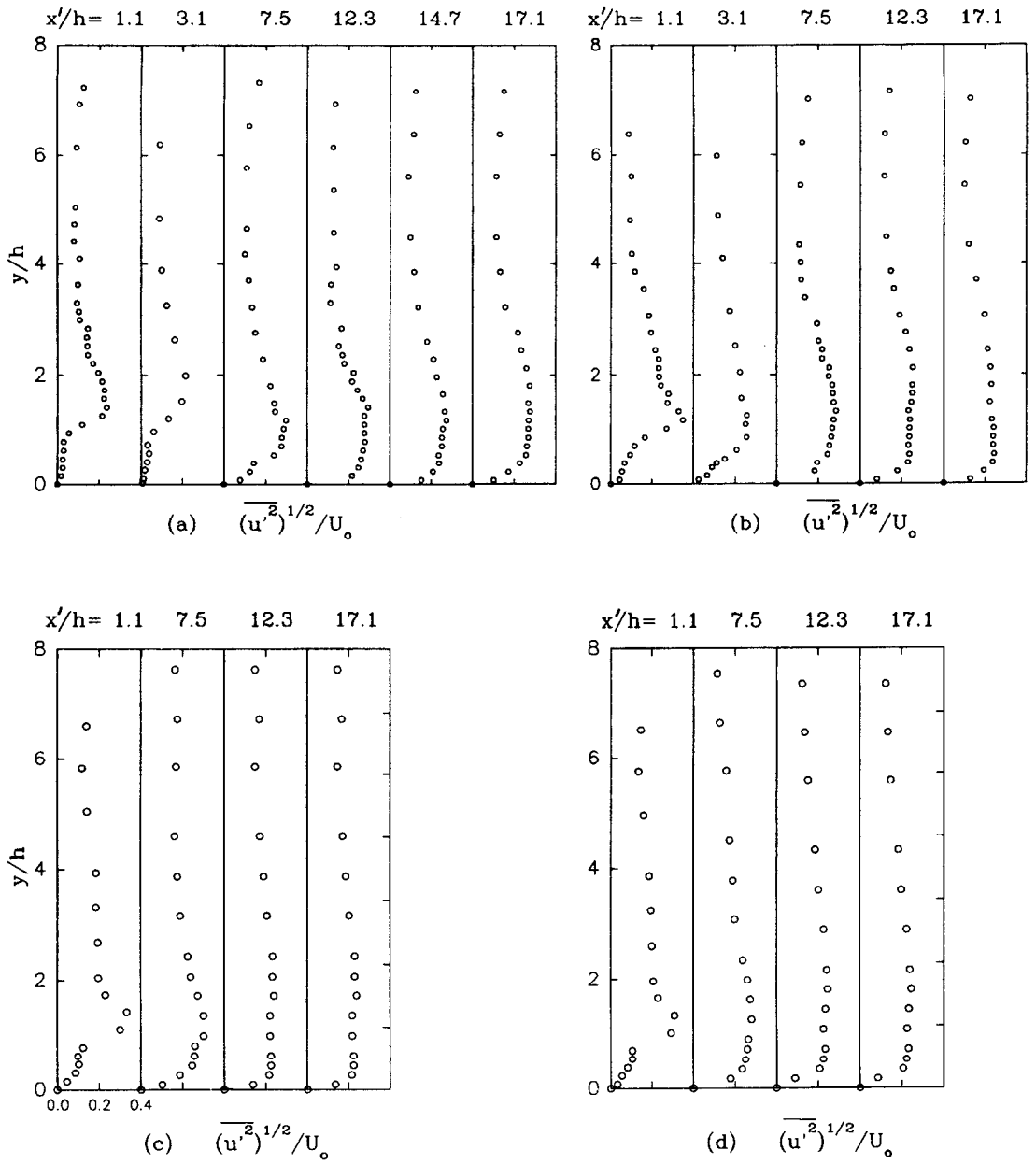

Fig. 7. Mean streamwise turbulence intensity profiles at $Re = 3400$: (a) between ribs 1 and 2; (b) between ribs 2 and 3; (c) between ribs 5 and 6; (d) between ribs 6 and 7.

reattachment occurs upstream of $x'/h = 5.7$. This is presumably due to the differences in the flow streamline curvature of the flow at the downstream face of the rib in the two interrib modules. Note that unlike the low-Re case, the turbulence levels in module 1 and the periodically developed regions are comparable (Figs. 12 and 14). Therefore, the decrease in reattachment length past the first module cannot be, in part, attributed to increases in the eddy diffusivity.

In the periodically developed regime, measurements are also reported above the rib, at $x'/h = 0$ corresponding to the downstream rib face and at $x'/h = -0.5$ corresponding to the mid-point of the rib. It is worth noting that the measured velocity closest to the rib surface is negative, indicating the presence of a small separation directly above the rib.

The streamwise turbulence intensity levels shown in Fig. 12 indicate, as noted above, that there is little increase in the turbulence level between the first and seventh interrib modules. These results, expected for flows that are initially fully turbulent, are in contrast with the previously described results at the lower Reynolds number. Also worth noting are the substantially higher levels of turbulence intensity in the first interrib

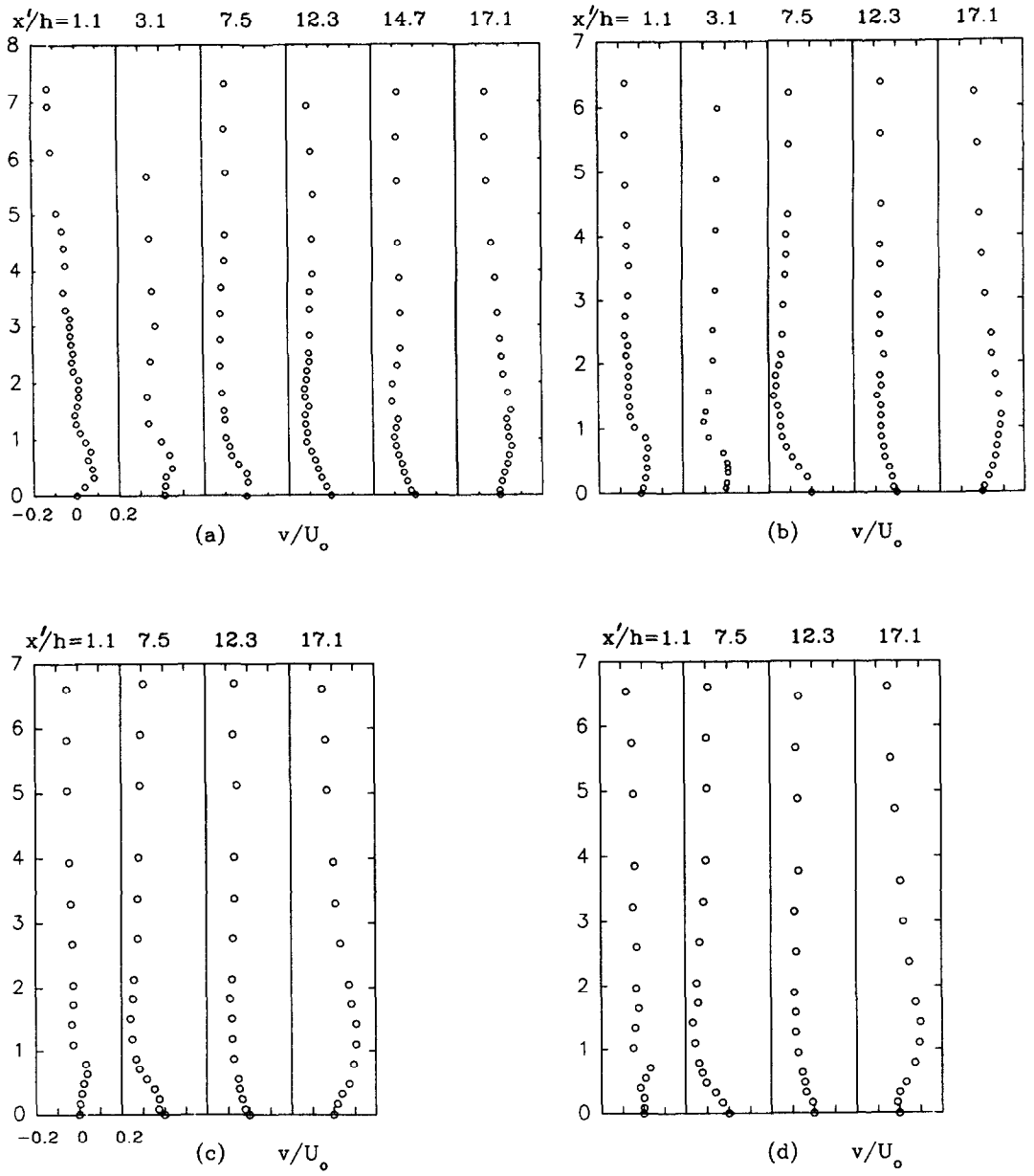

Fig. 8. Mean cross-stream velocity profiles at $Re = 3400$: (a) between ribs 1 and 2; (b) between ribs 2 and 3; (c) between ribs 5 and 6; (d) between ribs 6 and 7.

module at the higher Reynolds number, and the sudden decrease in the peak turbulence in the vicinity of reattachment, an observation previously noted for fully turbulent backstep flows [20]. The maximum streamwise turbulence intensity occurs at $x'/h = 0$, and not immediately downstream of the rib face, as would be expected based on backstep flow measurements [20].

The v velocities are presented in Fig. 13. A careful inspection of the v velocities in the corner behind the rib indicates a small counter-clockwise eddy beneath the primary clockwise eddy. This counter-rotating eddy is however, a relatively weak eddy, and does not appear to influence the heat transfer results (Fig. 3). The magnitude of the normalized v velocities appear to be comparable to those at the lower Reynolds number.

The cross-stream turbulence intensity profiles are shown in Fig. 14. Unlike the streamwise turbulence intensities, these profiles show an increase in the values of $\sqrt{\overline{v'^2}}/U_0$ with x'/h, with the maximum peak value ($\simeq 0.25$) occurring at $x'/h \cong 0.6$ and $y/h \cong 1$. These values, even in the first interrib module, are only slightly higher than the corresponding low-Re values

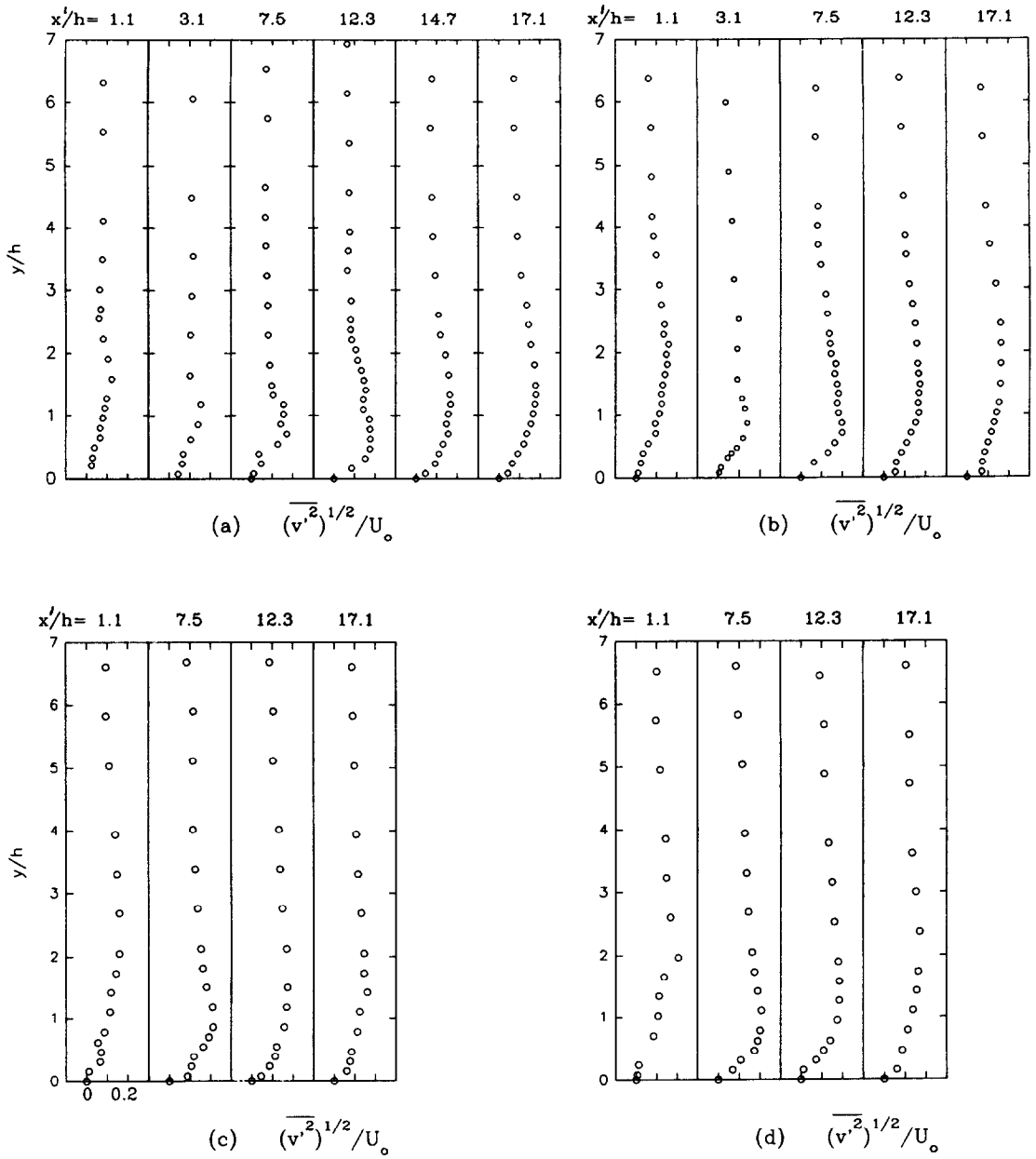

Fig. 9. Mean cross-stream turbulence intensity profiles at $Re = 3400$: (a) between ribs 1 and 2; (b) between ribs 2 and 3; (c) between ribs 5 and 6; (d) between ribs 6 and 7.

(in the 0.15–0.2 range). Recall that the values for the streamwise turbulence intensity at the higher Reynolds number were substantially higher in the first module than the corresponding values at $Re = 3400$, indicating the substantially higher level of anisotropy at $Re = 24\,000$.

The turbulent shear stress profiles (Fig. 15) indicate the relatively low values of the shear stress in the recirculation region, and the rapid increase in the shear-layer regions. The near-wall profiles begin to develop upstream of the point of reattachment, before $x'/h = 5.7$ in interrib module 1 and before $x'/h = 1.6$ in interrib module 7. Note that the peak shear stress values at the higher Reynolds number are typically much higher than that at $Re = 3400$, both in the developing region, just past the first rib, and in the periodically developed regions.

CONCLUDING REMARKS

Detailed measurements of the velocity, temperature, and heat transfer fields were performed in a

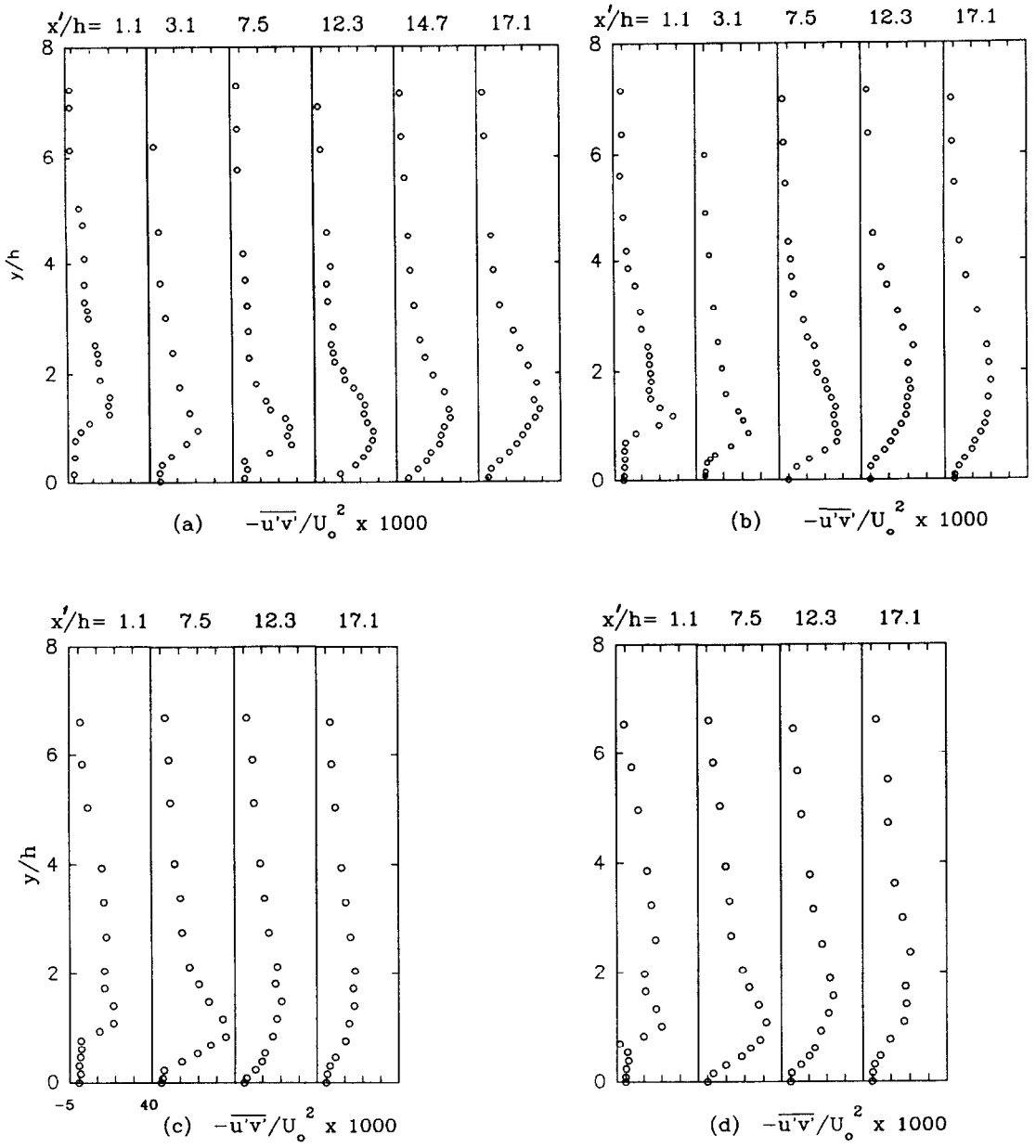

Fig. 10. Mean turbulent shear stress profiles at $Re = 3400$: (a) between ribs 1 and 2; (b) between ribs 2 and 3; (c) between ribs 5 and 6; (d) between ribs 6 and 7.

ribbed duct for two inlet flow conditions: a transitional flow at a $Re = 3400$, and a fully turbulent flow at a $Re = 24\,000$. The development of the heat transfer field for the fully turbulent inlet flow shows the expected decay of the interrib Nusselt number profiles to the periodic state. For the incoming transitional flow, the Nusselt numbers in the second interrib module are higher than those in the first, indicating the effect of the flow transition to fully turbulent flow. Beyond the second rib, the interrib profiles again decay to the periodic state. Transition to the fully turbulent state appears to occur in the vicinity of reattachment after the first rib.

The measured velocity and temperature fields appear to confirm the above noted transition and associated heat transfer behavior. At $Re = 3400$, a significant increase (nearly twofold) in the streamwise turbulence intensity is noted after the second rib to levels comparable to those in the periodically developed regions. The corresponding increases in the cross-stream intensity and shear stress are smaller. At $Re = 24\,000$, there is practically no increase in the

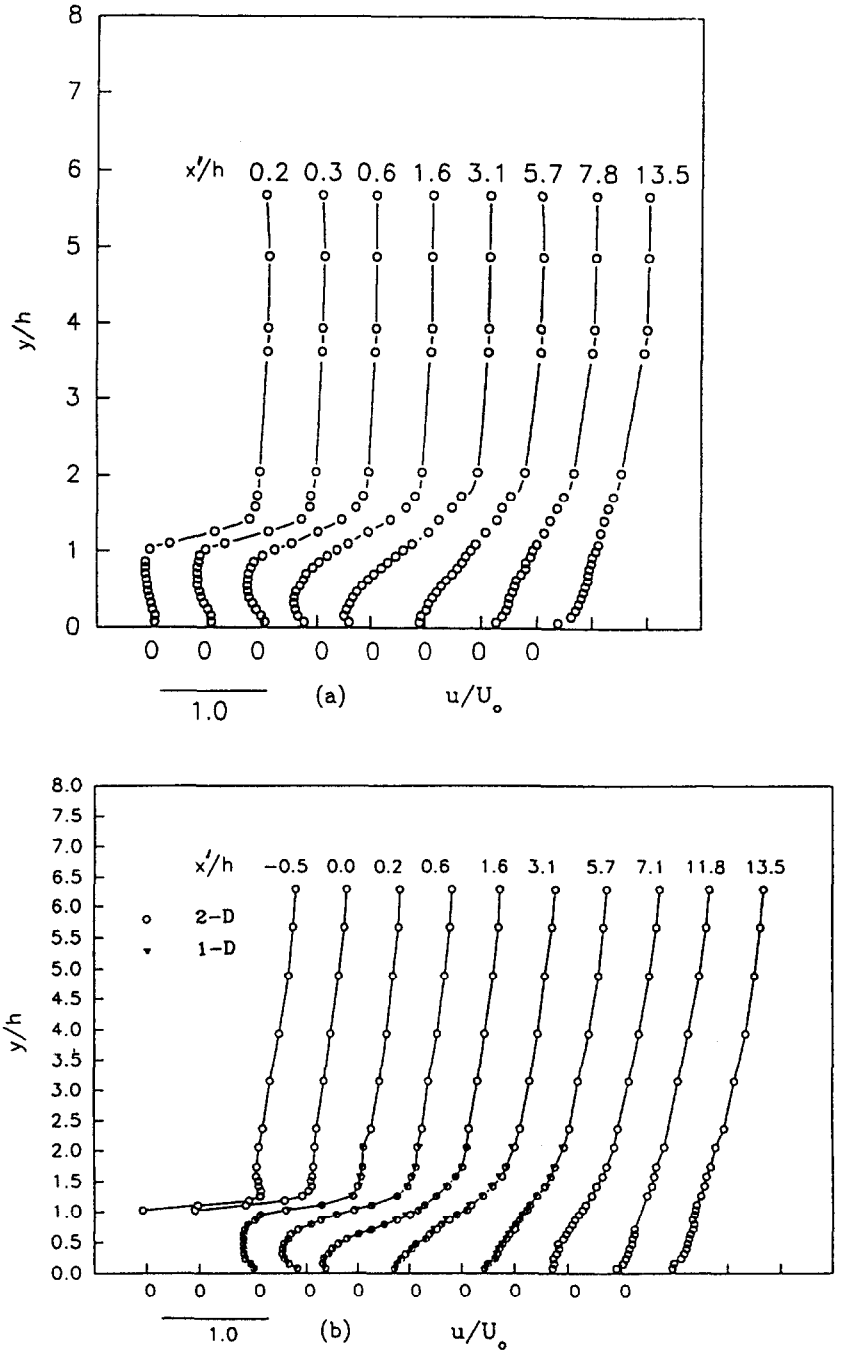

Fig. 11. Mean streamwise velocity profiles at $Re = 24000$: (a) between ribs 1 and 2; (b) between ribs 7 and 8.

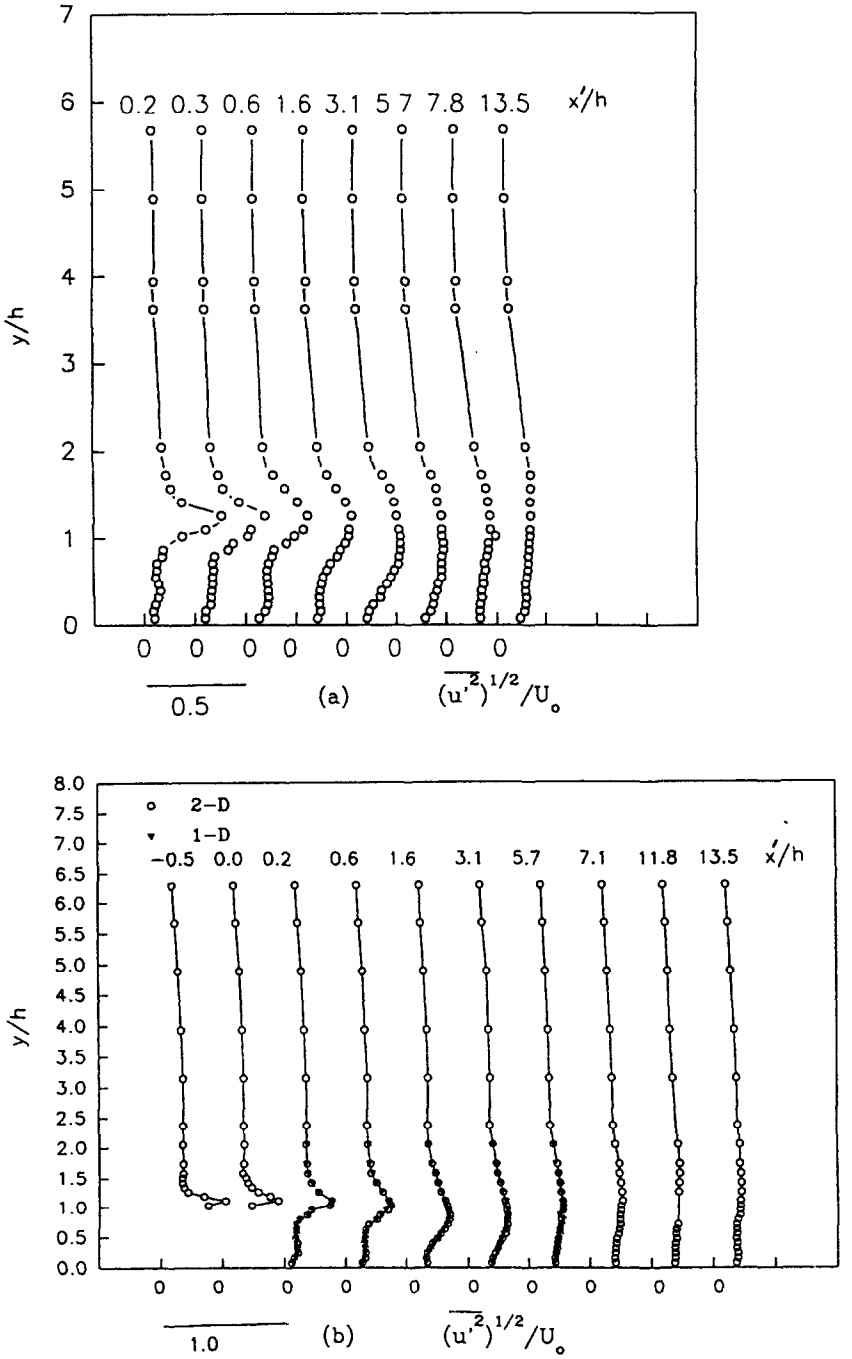

Fig. 12. Mean streamwise turbulent intensity profiles at $Re = 24000$: (a) between ribs 1 and 2; (b) between ribs 7 and 8.

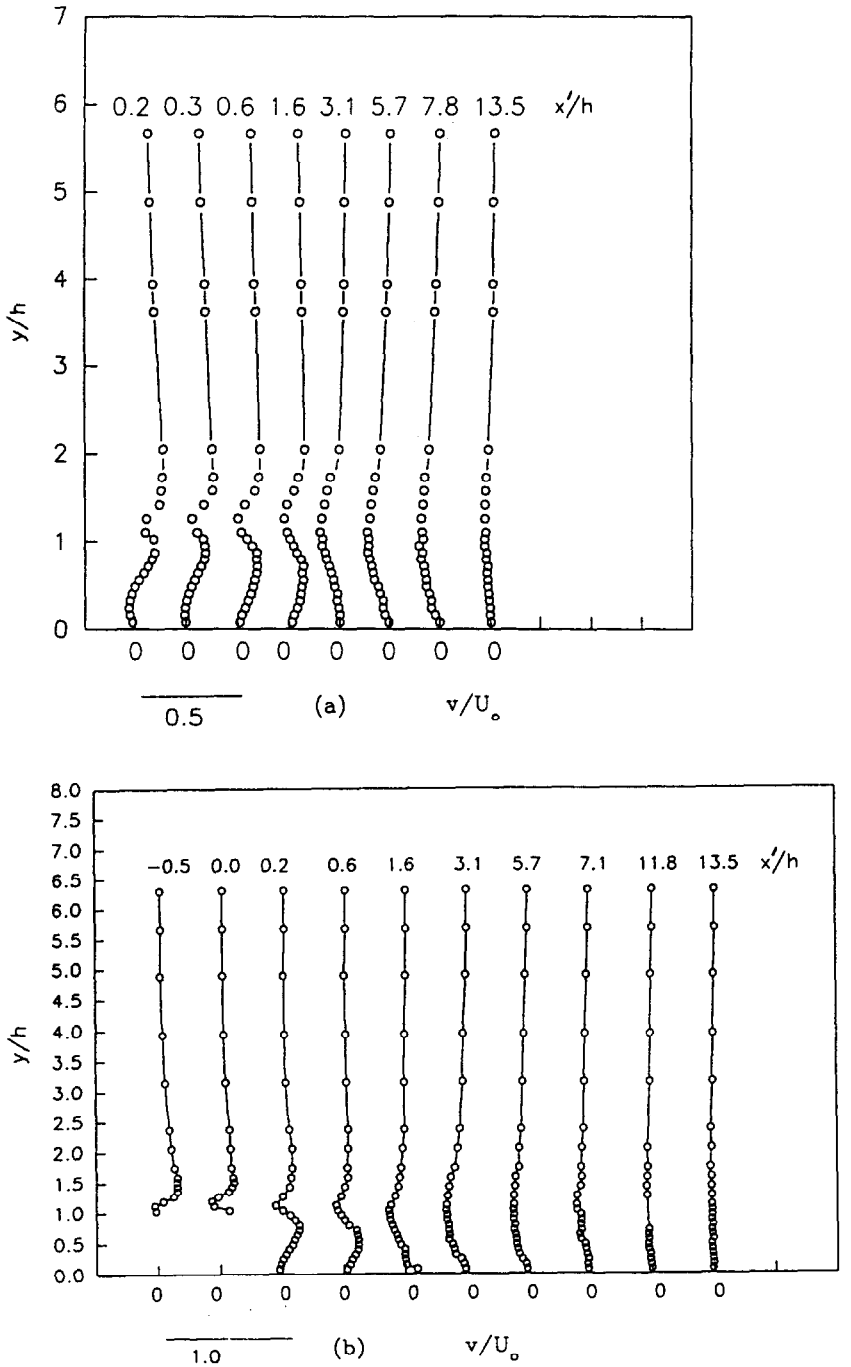

Fig. 13. Mean cross-stream velocity profiles at $Re = 24\,000$: (a) between ribs 1 and 2; (b) between ribs 7 and 8.

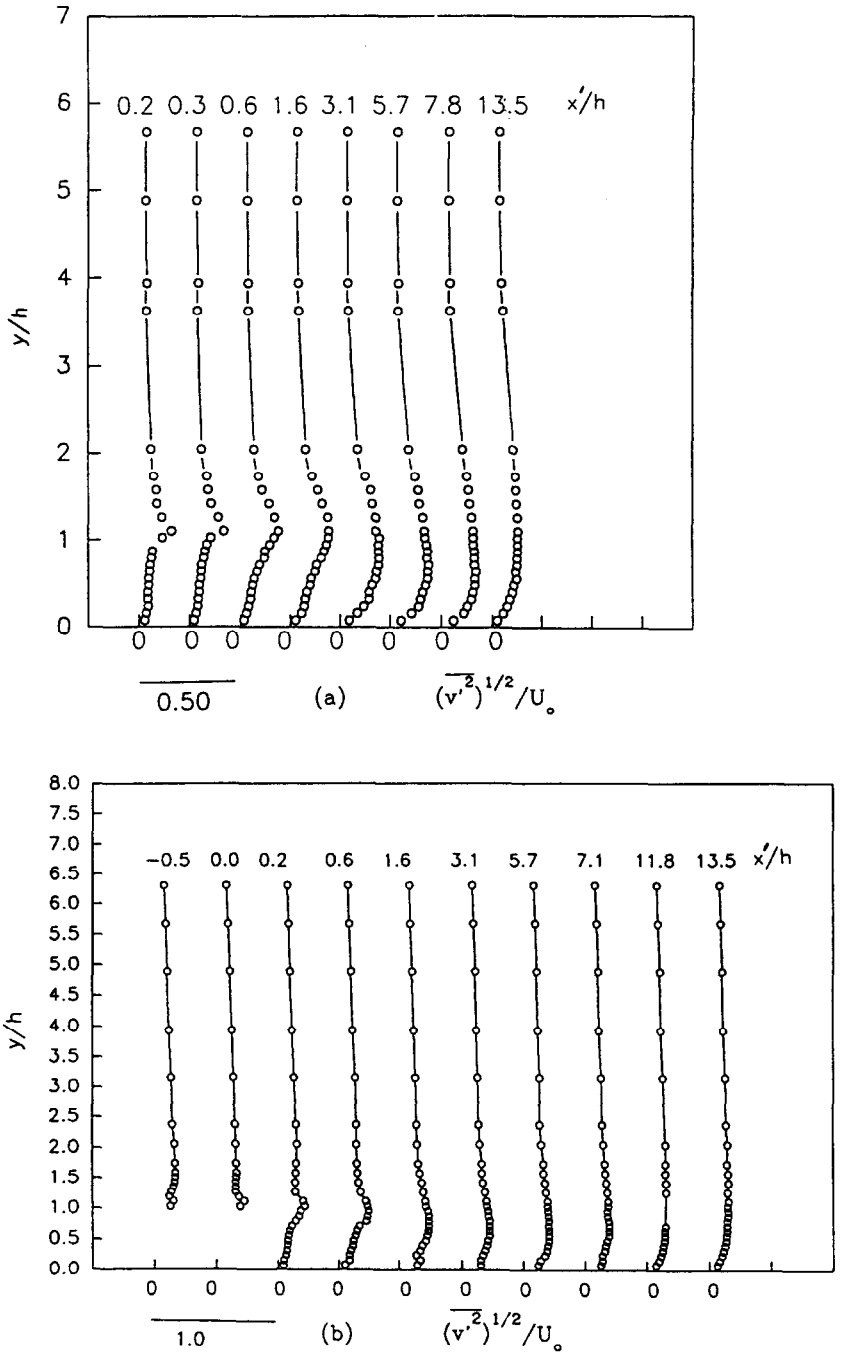

Fig. 14. Mean cross-stream turbulent intensity profiles at $Re = 24\,000$: (a) between ribs 1 and 2; (b) between ribs 7 and 8.

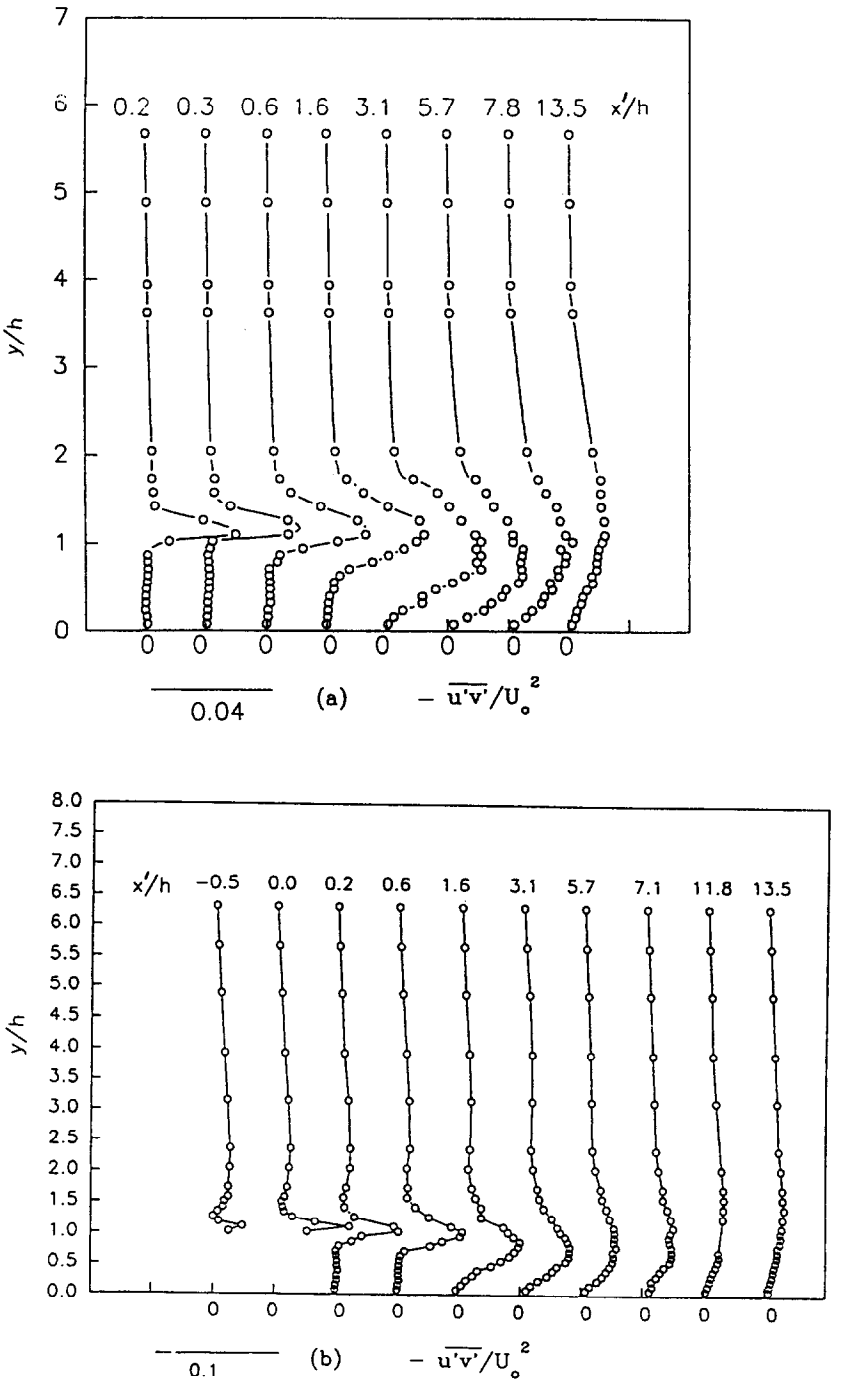

Fig. 15. Mean turbulent shear stress profiles at $Re = 24000$: (a) between ribs 1 and 2; (b) between ribs 7 and 8.

streamwise and cross-stream turbulence intensity between the first and the seventh interrib module. In the fully turbulent regions, the turbulence levels peak at or downstream of the rib and decay with streamwise distance. In the vicinity of reattachment there is a sudden decrease in the turbulence levels. However, in the first interrib module for $Re = 3400$ the turbulence levels increase downstream of the flow separation and

peak in the vicinity of reattachment, where transition to fully turbulent flow is completed.

Acknowledgements—This work was supported by a grant from the National Science Foundation (CTS-8800736) and a grant by the Gas Research Institute (GRI-5090-260-1961). Their support is gratefully acknowledged.

REFERENCES

1. F. Durst, M. Founti and S. Obi, Experimental and computational investigation of the two-dimensional channel flow over two fences in tandem, *J. Fluids Engng* **110,** 48–54 (1988).
2. T. M. Liou, Y. Chang and D. W. Hwang, Experimental and computational study of turbulent flows in a channel with two pairs of turbulence promoters in tandem, *J. Fluids Engng* **112,** 302–310 (1990)
3. T. M. Liou and T. J. Hwang, Turbulent heat transfer augmentation and friction in periodic fully developed channel flows, *J. Heat Transfer* **114,** 56–64 (1992).
4. L. E. Drain and S. Martin, Two-component velocity measurements of turbulent flow in a ribbed-wall flow channel, *International Conference on Laser Anemometry-Advances and Application*, Manchester, pp. 99–112 (1985).
5. H. Yokosawa, H. Hijita, M. Hirota and S. Iwata, Measurement of turbulent flow in a square duct with roughened walls on two opposite sides, *Int. J. Heat Fluid Flow* **10,** 125–130 (1989).
6. S. Acharya, S. Dutta, T. A. Myrum and R. S. Baker, Periodically developed flow and heat transfer in a ribbed duct, *Int. J. Heat Mass Transfer* **36,** 2069–2082 (1993).
7. J. F. Lockett and M. F. Collins, Holographic interferometry and its applications to turbulent convective heat transfer, *Int J. Heat Mass Transfer* **33,** 2439–2449 (1990).
8. E. M. Sparrow and W. Q. Tao, Enhanced heat transfer in a flat rectangular duct with streamwise periodic disturbances at one principal wall, *J. Heat Transfer* **105,** 851–861 (1983).
9. J. C. Han, Heat transfer and friction in channels with two opposite rib-roughened walls, *J. Heat Transfer* **106,** 774–781 (1984).
10. J. C. Han, Heat transfer and friction in channels with rib turbulators, *J. Heat Transfer* **110,** 321–328 (1988).
11. T. M. Liou and J. J. Hwang, Developing heat transfer and friction in a ribbed rectangular duct with flow separation at inlet, *J. Heat Transfer* **114,** 565–573 (1992).
12. T. M. Liou, J. J. Hwang and S. H. Chen, Simulation and measurement of enhanced turbulent heat transfer in a channel with periodic ribs in one principal wall, *Int. J. Heat Mass Transfer* **36,** 507–517 (1993).
13. D. A. Aliaga, J. P. Lamb and D. E. Klein, Convection heat transfer distributions over plates with square ribs from infrared thermography measurements, *Int. J. Heat Mass Transfer* **37,** 363–374 (1994).
14. D. M. Driver and H. L. Seegmiller, Features of a reattaching shear layer subject to adverse pressure gradient, *AIAA*-82-10290, *AIAA/ASME 3rd Joint Thermophysics, Fluids and Heat Transfer Conference*, St. Louis, MO (1982).
15. D. M. Driver and H. L. Seegmiller, Features of a reattaching turbulent shear layer in divergent channel flow, *AIAA J.* **23,** 163–171 (1985).
16. S. J. Kline and F. A. McClintock, Estimating uncertainty in single sample experiments, *Mech. Engng* **75,** 3–8 (1953).
17. E. P. Rood and D. P. Telionis, Journal of fluids engineering policy on reporting uncertainties in experimental measurements and results, *J. Fluids Engng* **113,** 313–314 (1991).
18. D. E. Coles and E. A. Hirst, *Proceedings Computation of Turbulent Boundary Layers*, 1962, AFOSR-IFP, *Stanford Conference*, Vol. 2 (1968).
19. S. Acharya, S. Dutta, T. A. Myrum and S. Baker, Turbulent flow past a surface mounted two-dimensional rib, *J. Fluids Engng* **116,** 238–246 (1994).
20. C. Chandrasuda and P. Bradshaw, Turbulence structure of a reattaching mixing layer, *J. Fluid Mech.* **110,** 171–194 (1981).